Heat Transfer in Gas Turbine Combustors

Maria da Graça Carvalho* and Pedro Jorge Coelho†
Instituto Superior Técnico, Lisbon, Portugal

The present paper is concerned with the prediction of the local flow, heat-transfer, and combustion processes inside a three-dimensional can combustor chamber of a gas turbine. A three-dimensional numerical solution technique is used to solve the governing time-averaged partial differential equations and the physical modeling for turbulence, combustion, and thermal radiation. Heat-transfer modeling is emphasized in this paper. A method to calculate the distribution of temperature, radiative heat flux, and total heat flux of the liner is described. The implications of neglecting radiative heat transfer in gas turbine combustion chamber calculations are discussed. The influence of working pressure on radiative heat transfer is investigated, comparing the radiative heat flux and temperature distribution of the liner for three different working pressures: 5, 15, and 25 bar. Both radiative and convective fluxes increase with pressure, mainly because of the increase of inlet air temperature and gas emissivity. The ratio of the fluxes to the energy supplied to the combustor is very small. However, the accurate assessment of the flux distribution is an essential prerequisite for the prediction of the liner temperature distribution and liner life.

Nomenclature

C_f = soot formation rate coefficient
C_{g1}, C_{g2} = constants in combustion model
C_{pj} = constant pressure specific heat of species j
C_μ = constants in turbulence model
C_1, C_2 = constants in turbulence model, Eq. (7); also convection fluxes, Eq. (13)
f = mixture fraction
G_k = generation of turbulent kinetic energy
g = time-averaged mixture fraction fluctuations
h = specific enthalpy
H_j = lower calorific value of species j
k = kinetic energy of turbulence
K_{12} = conduction heat transfer through the liner
M_j = molecular weight of species j
m_j = time-averaged mass function of species j
$P(\hat{f})$ = probability density function of mixture fraction
p = pressure
R_0 = universal gas constant
R_1, R_2 = radiation fluxes
r = radial coordinate
T = temperature
u = time-averaged velocity component in the x direction
v = time-averaged velocity component in the r direction
w = time-averaged velocity component in the θ direction
x = axial coordinate
ε = dissipation rate of turbulent kinetic energy
θ = tangential coordinate
μ_t = turbulent viscosity
ρ = time-mean density
σ_ϕ = Prandtl or Schmidt number for the variable ϕ
τ_{ij} = combined laminar and turbulent stresses
ϕ = generic property

Superscript

$(\hat{\ })$ = instantaneous value

Subscript

1 = flame side of liner wall, Eq. (13)
2 = coolant side of liner wall, Eq. (13)
Fu = fuel

Received Nov. 30, 1987; revision received April 18, 1988.

*Associate Professor, Department of Mechanical Engineering.
†Research Assistant, Department of Mechanical Engineering.

Introduction

FOR many years, the design of gas turbine combustion chambers was based on the use of empirical models correlating overall performance with simple global parameters such as inlet air conditions, fuel/air ratio, or chamber volume. However, in the last two decades, awareness of the limitations of energy resources, on one hand, and pollutant emissions regulations, on the other, have imposed additional constraints, leading to the need to optimize the design of combustion equipment, including gas turbine combustors. Together with these limitations, all combustors should satisfy the following requirements: high combustion efficiency, uniformity of outlet gas temperature to maximize the life of turbine blades and nozzle guide vanes, wide stability limits, low pressure loss, reliable and smooth ignition, durability, and minimum cost.[1]

The improvement of the performance and the need to satisfy all of the listed requirements cannot be achieved by traditional methods. With these methods, spatial variations in dependent variables such as velocity and temperature are largely ignored, and no attempt is made at calculating the local detailed features of the flow, reaction, and heat transfer. An alternative and much more powerful approach is that based on the use of the finite-difference solution of the averaged forms of the partial differential conservation equations for momentum, mass, chemical species, and energy.

Calculation methods for practical combustion systems based on the finite-difference solution of the three-dimensional forms of the conservation equations have become viable in the past few years. These calculation methods have been used to predict the flow and combustion to gas turbine combustors by Jones et al.,[2] Jones and Priddin,[3] Jones and McGuirk,[4] and Coupland and Priddin.[5] Because of the multiplicity of phenomena involved, these works did not consider radiative heat transfer. However, in gas turbine combustion chambers, a large proportion of the total heat flux to the liner walls is by radiation from the flame. This radiant heating poses serious problems regarding liner durability. To ensure a satisfactory liner life, it is important to keep temperatures and temperature gradients down to an acceptable level. To supplement the removal of

heat from the liner, a film of cool air along the inner surface of the liner is usually provided. This problem is particularly severe for high pressure ratios, because the increase in pressure raises the amount of radiative heat transfer to the liner walls and the cooling of the walls by convection will be less effective due to the higher temperature of the inlet combustion air temperature. For such pressures, a high percentage of the total combustor airflow is used in film cooling the liner, which deteriorates the temperature pattern factor at the combustor exit, reduces the combustion efficiency, and increases the emissions of carbon monoxide and unburned hydrocarbons. Therefore, it is important to develop accurate predictive tools that will enable improved efficiency of cooling techniques.

Current interest and legislation concerning the reduction of combustion-generated pollutant emissions have imposed additional constraints on the conventional design practice.

The accurate assessments of pollutant emissions necessitate fairly precise knowledge of radiant heat-transfer rates because the models for predicting the emissions of carbon monoxide, unburned hydrocarbons, and oxides of nitrogen require an accurate description of gas temperature distributions in all regions of the combustor.[6] In addition, over the past 30 years, pressure ratios have increased markedly in order to improve thermal efficiency, and it seems probable that they will continue to do so. This increase in pressure raises the amount of heat transferred to the liner walls by radiation.

Despite its considerable practical importance, the process of flame radiation in gas turbine combustors has not been subject to extensive investigation.

Boysan et al.[7] used a flux model to account for the effects of radiation in a gas turbine combustor solving three second-order linear differential equations for the fluxes in the axial, radial, and tangential directions. The contribution of radiation was considered in the enthalpy equation through a source term calculated from those fluxes. The study was carried out at atmospheric pressure. The authors did not specify the type of boundary condition used for the calculation of the radiation heat transfer, nor did they discuss its influence on the results.

Sampath and Ganesan[8] used the same flux model to compute radiation heat transfer in a gas turbine combustor. However, heat transfer was not the aim of the investigation and, therefore, predictions of heat fluxes were not presented.

Lockwood et al.[9] used the "discrete transfer" radiation prediction procedure of Lockwood and Shah[10] for the computation of the radiation transfer in a combustor can. The authors assumed adiabatic flame and did not solve for the enthalpy equation. The distribution of temperature was determined as a function of the instantaneous mixture fraction using the equilibrium method of Gordon and McBride.[11] Therefore, the effects of radiative heat transfer on the flow, temperature field, and chemical reaction were not accounted for. The radiative heat fluxes to the walls were calculated a posteriori assuming a uniform wall temperature equal to the inlet air temperature. They have concluded that the total radiation heat transfer to the walls was less than 0.25% of the energy supplied to the combustor, justifying the adiabatic assumption on which the flow and reaction calculations were based.

Carvalho et al.[12] performed a study similar to that of Lockwood et al.,[9] also using the discrete transfer method for the prediction of radiative heat transfer in a can combustor. In this case, however, the authors solved the enthalpy equation with a source term accounting for the heat transferred by radiation. The wall temperature was assumed uniform and equal to the inlet air temperature. Two sets of predictions were made for pressures of 6 and 25 bar. Radiative wall heat fluxes increased markedly with the pressure.

In the present paper, the discrete transfer method of Lockwood and Shah[10] is also used. The principal contribution of this paper is the calculation of the wall temperature distribution that was assumed in the previous works. In order to calculate the wall temperature distribution, we use, for the calculation of the radiative heat transfer, a boundary condition based on the energy balance of the wall, similar to the one described by Lefebvre.[1] This balance is applied to each control volume adjacent to the wall, and it is based on 1) empirical correlations for the calculation of external convection and radiation, 2) the wall law for the calculation of internal convection, and 3) the discrete transfer method for the calculation of internal radiation. The enthalpy equation is solved, and a source term accounting for the radiation heat transfer is included. Instantaneous gas compositions are determined as a function of the instantaneous mixture fraction using the equilibrium method of Gordon and McBride.[11]

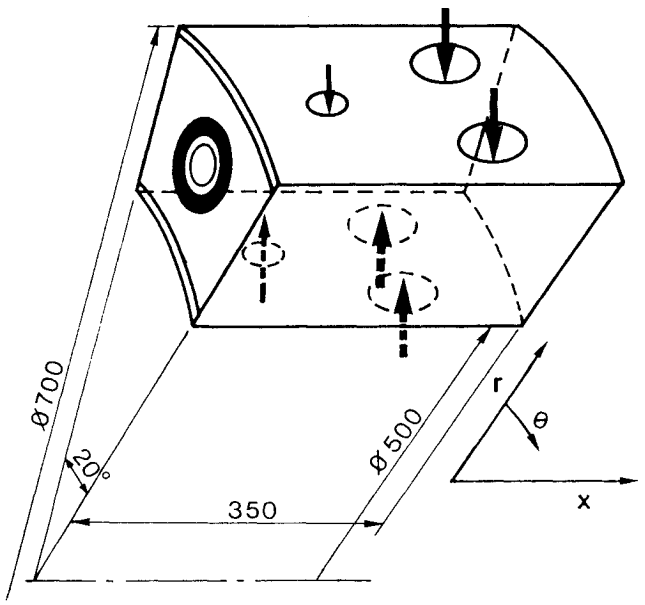

Fig. 1 Annular combustor geometry.

Predictions of wall temperature, radiative heat flux, and total heat flux distributions are presented and discussed. The influence of the pressure ratio is analyzed, comparing the solutions obtained for three different working pressures: 5, 15, and 25 bar.

Flow Configuration

The geometry of the combustion chamber studied is sketched in Fig. 1. The combustor has 18 separated burners. Because the combustor geometry repeats itself every 20 deg along with the flow pattern, only a single 20-deg section of the chamber is studied. Gaseous fuel (propane) enters the combustor through the inner of two annular rings. It was assumed to enter in the form of a conical jet of 90-deg included angle. The combustion air is introduced through a concentric annular ring. Two streams of cooling air enter close to the inner and outer annulus walls, simulating the cooling ring flows, which actually are discharged parallel to the walls. Intermediate and dilution air are introduced through round holes in the inner and outer annulus walls, as shown in Fig. 1. The air has been specified as entering only with a radial velocity component through the holes. Three sets of operating conditions were studied, keeping an overall air/fuel ratio of approximately 60 and varying combustor pressure (see Table 1). Since an increase in pressure from case 1 to case 3 results from an increase in the compressor's pressure ratio, the inlet air temperature and mass flow rates must also increase.

Physical Modeling

The governing transport equations for the mean motion of a turbulent three-dimensional flow were applied in cylinder polar

Table 1 Operating conditions

	Case 1	Case 2	Case 3
Pressure, bar	5	15	25
Inlet air temperature, K	400	600	750
Inlet fuel temperature, K	300	400	500
Primary air mass flow rate, kg/s	0.233	0.466	0.621
Cooling air mass flow rate, kg/s	0.146	0.292	0.398
Intermediate air mass flow rate through the holes, kg/s	0.114	0.227	0.304
Dilution air mass flow rate through the holes, kg/s	0.172	0.341	0.456
Mass flow rate of fuel, kg/s	0.011	0.022	0.0295
Primary air axial inlet velocity, m/s	40	40	40
Fuel axial inlet velocity, m/s	25	22.2	22.2

coordinate form as follows:

Continuity:

$$\frac{1}{r}\frac{\partial}{\partial r}(\rho r v)+\frac{1}{r}\frac{\partial}{\partial \theta}(\rho w)+\frac{\partial}{\partial x}(\rho u)=0 \tag{1}$$

Momentum:

$$\rho\left(v\frac{\partial v}{\partial r}+\frac{w}{r}\frac{\partial v}{\partial \theta}-\frac{w^2}{r}+u\frac{\partial v}{\partial x}\right)=-\frac{\partial p}{\partial r}-\left[\frac{1}{r}\frac{\partial}{\partial r}(r\tau_{rr})+\frac{1}{r}\frac{\partial}{\partial \theta}\tau_{r\theta}-\frac{\tau_{\theta\theta}}{r}+\frac{\partial \tau_{rx}}{\partial x}\right] \tag{2}$$

$$\rho\left(v\frac{\partial w}{\partial r}+\frac{w}{r}\frac{\partial w}{\partial \theta}+\frac{vw}{r}+u\frac{\partial w}{\partial x}\right)=-\frac{1}{r}\frac{\partial p}{\partial \theta}-\left[\frac{1}{r^2}\frac{\partial}{\partial r}(r^2\tau_{r\theta})+\frac{1}{r}\frac{\partial \tau_{\theta\theta}}{\partial \theta}+\frac{\partial \tau_{\theta x}}{\partial x}\right] \tag{3}$$

$$\rho\left(v\frac{\partial u}{\partial r}+\frac{w}{r}\frac{\partial u}{\partial \theta}+u\frac{\partial u}{\partial x}\right)=-\frac{\partial p}{\partial x}-\left[\frac{1}{r}\frac{\partial}{\partial r}(r\tau_{rx})+\frac{1}{r}\frac{\partial}{\partial \theta}(\tau_{\theta x})+\frac{\partial}{\partial x}(\tau_{xx})\right] \tag{4}$$

Here v, w, and u represent the velocities in the (r,θ,x) cylindrical-coordinate directions; and ρ and p are the density and pressure, respectively. The combined laminar and turbulent stresses are represented by τ; these are supposed to be related to velocity gradients by way of an isotropic effective viscosity $\mu_{\text{eff}}=\mu+\mu_t$, where μ is the laminar viscosity and μ_t is the turbulent viscosity derived at each point from

$$\mu_t=C_\mu \rho k^2/\varepsilon \tag{5}$$

where C_μ is a constant of the model, and k and ε are derived from their differential transport equations. The turbulence kinetic energy equation is

$$\rho\left(v\frac{\partial k}{\partial r}+\frac{w}{r}\frac{\partial k}{\partial \theta}+u\frac{\partial k}{\partial x}\right)=\frac{1}{r}\frac{\partial}{\partial r}\left(r\frac{\mu_t}{\sigma_k}\frac{\partial k}{\partial r}\right)+\frac{1}{r}\frac{\partial}{\partial \theta}\left(\frac{\mu_t}{\sigma_k}\frac{\partial k}{r\partial \theta}\right)+\frac{\partial}{\partial x}\left(\frac{\mu_t}{\sigma_k}\frac{\partial k}{\partial x}\right)+G_k-\rho\varepsilon \tag{6}$$

where σ_k is another universal turbulence constant, and G represents the volumetric rate of generation of k and can be expressed in terms of velocity gradients and the turbulent viscosity. The dissipation-rate equation is

$$\rho\left(v\frac{\partial \varepsilon}{\partial r}+\frac{w}{r}\frac{\partial \varepsilon}{\partial \theta}+u\frac{\partial \varepsilon}{\partial x}\right)=\frac{1}{r}\frac{\partial}{\partial r}\left(r\frac{\mu_t}{\sigma_\varepsilon}\frac{\partial \varepsilon}{\partial r}\right)+\frac{1}{r}\frac{\partial}{\partial \theta}\left(\frac{\mu_t}{\sigma_\varepsilon}\frac{\partial \varepsilon}{r\partial \theta}\right)+\frac{\partial}{\partial x}\left(\frac{\mu_t}{\sigma_\varepsilon}\frac{\partial \varepsilon}{\partial x}\right)+C_1\frac{\varepsilon}{k}G_k-C_2\frac{\rho\varepsilon^2}{k} \tag{7}$$

where C_1, C_2, and σ_ε are all turbulence constants.

The model constants appearing in the preceding equations were assigned the following values, taken unchanged from Launder and Spalding[13]: $C_\mu=0.9$, $C_1=1.44$, $C_2=1.92$, $\sigma_k=1.0$, and $\sigma_\varepsilon=1.3$.

The combustion model is based on the assumption that the reaction rates associated with the fuel oxidation have time scales that are very short compared with those describing the transport processes. Using the assumption of "fast" chemical reaction, chemical equilibrium prevails. Assuming also that all species and heat diffuse at the same rate and that the heat loss to the surroundings can be neglected compared with the heat transfer released by chemical reaction, then instantaneous gas composition can be determined as a function of a strictly conserved scalar variable. Any conserved scalar may be chosen; here we used the mixture fraction f defined as the mass fraction of fuel present both burned and unburned. Instantaneous gas composition was determined from f using an equilibrium model based on the minimization of the free energy.[11] The version of the equilibrium model used is identical to that used by Godoy.[14] In this version of the model, a rich flammability limit at an equivalence ratio of 2.5 was introduced. The instantaneous temperature field was calculated from the instantaneous enthalpy field, which was correlated with the instantaneous mixture fraction field assuming the relations used by Carvalho.[15]

In a turbulent flow, the mixture fraction will fluctuate and, because of the nonlinearity of the relationships, knowledge of its mean value is insufficient to allow the determination of the mean values of such quantities as density, and temperature. We adopt a statistical approach to describe the temporal nature of the mixture fraction fluctuations. The time-averaged value of any property ϕ solely dependent on f then can be determined from

$$\phi=\int_0^1 \phi(\hat{f})P(\hat{f})\,d\hat{f} \tag{8}$$

In the present work, we have assumed the "clipped normal" probability density function,[16] which is defined completely by the knowledge of the mean value of the mixture fraction f and its variance g. Variables f and g also obey modeled transport equations of the form

$$\rho\left(v\frac{\partial f}{\partial r}+\frac{w}{r}\frac{\partial f}{\partial \theta}+u\frac{\partial f}{\partial x}\right)=\frac{1}{r}\frac{\partial}{\partial r}\left(r\frac{\mu_t}{\sigma_f}\frac{\partial f}{\partial r}\right)+\frac{1}{r}\frac{\partial}{\partial \theta}\left(\frac{\mu_t}{\sigma_f}\frac{\partial f}{r\partial \theta}\right)+\frac{\partial}{\partial x}\left(\frac{\mu_t}{\sigma_f}\frac{\partial f}{\partial x}\right) \tag{9}$$

$$\rho\left(v\frac{\partial g}{\partial r}+\frac{w}{r}\frac{\partial g}{\partial \theta}+u\frac{\partial g}{\partial x}\right)=\frac{1}{r}\frac{\partial}{\partial r}\left(r\frac{\mu_t}{\sigma_g}\frac{\partial g}{\partial r}\right)+\frac{1}{r}\frac{\partial}{\partial \theta}\left(\frac{\mu_t}{\sigma_g}\frac{\partial g}{r\partial \theta}\right)+\frac{\partial}{\partial x}\left(\frac{\mu_t}{\sigma_g}\frac{\partial g}{\partial x}\right)+Cg_1\mu_t\left[\left(\frac{\partial f}{\partial x}\right)^2+\left(\frac{\partial f}{\partial r}\right)^2+\left(\frac{1}{r}\frac{\partial f}{\partial \theta}\right)^2\right]-\frac{Cg_2}{k}\rho\varepsilon g \tag{10}$$

where Cg_1 and Cg_2 are additional adjustable parameters.

The mixture specific enthalpy may be defined by

$$h\equiv\int_0^T\sum_{\text{all }j} m_j C_{pj}(T)\,dT+m_{fu}H_{fu}+m_{\text{CO}}H_{\text{CO}}+m_{\text{H}_2}H_{\text{H}_2} \tag{11}$$

where C_{pj} is the constant-pressure specific heat of species j.

Density is determined from the equation of state

$$\rho = p\left(R_0 T \sum_{\text{all}_j} m_j/M_j\right)^{-1} \tag{12}$$

where p is the pressure, R_0 the universal gas constant, and M_j the molecular weight of species j. Since m_j as well as T are functions of f, the time-averaged density for use in the mean flow equations is again determined from Eq. (8).

Treatment of the Radiation Transfer

The discrete transfer radiation prediction procedure of Lockwood and Shah[10] has been used in this study. The calculated energy sources are appended to the energy balance equation solved for by the flow code.

The gas-absorption coefficient is calculated from the "two grey plus a clear gas" fit of Truelove.[17] Water vapor and carbon dioxide are the prime contributors to the gaseous radiation. The contribution of the carbon monoxide and fuel for the gas-absorption coefficient was not considered because of the lack of appropriate data. However, it is thought that the total combustor absorption by the fuel and carbon monoxide will be small.

We have made no attempt to solve for the soot. The process governing the rates of formation and the subsequent oxidation of soot are highly complex, and quantitative models to describe these processes, are not yet fully developed.[6] The fuel considered in the present application, propane, has a high hydrogen content displaying a low propensity toward soot formation (see Naegeli et al.[18]).

The boundary condition necessary for the calculation of the radiative heat transfer was obtained from an energy balance of the liner as suggested in Ref. 1. Broadly, the liner is heated by radiation and convection from the hot gases inside it; it is cooled by radiation to the outer casing and by convection to the annulus air. Under equilibrium conditions, the liner temperature is such that the internal and external heat fluxes at any point are just equal. Loss of heat by conduction along the liner wall is comparatively small and usually may be neglected. Since the liner wall is usually very thin, we have neglected the difference between the inner and outer liner wall areas. The cooling holes are assumed to be black surfaces in which temperature is the inlet air temperature. Therefore, under steady-state conditions, the following balance equation can be written:

$$R_1 + C_1 = R_2 + C_2 = K_{12} \tag{13}$$

where subscript 1 refers to internal fluxes, subscript 2 to external fluxes, and K_{12} the conduction heat transfer through a solid liner wall due to a temperature gradient within the wall. Internal radiation R_1 is calculated using the discrete transfer model, while the internal convection C_1 was calculated from Reynolds analogy (see, for example, Ref. 19). Calculations of external radiation and convection, R_2 and C_2, were done using the correlations presented by Lefebvre.[1]

The calculation procedure may be summarized as follows:

1) As a first guess, the liner wall temperature (flame side) is assumed to be equal to the inlet air temperature.

2) The internal radiation R_1 and internal convection C_1 are calculated.

3) Using the relationship $R_1 + C_1 = R_2 + C_2$, the liner wall temperature (coolant side) is calculated. A nonlinear equation has to be solved because R_2 is proportional to T^4. The Newton-Raphson method was used for the solution of this equation.

4) Setting $R_1 + C_1 = K_{12}$, a new value for the liner wall temperature (flame side) is obtained, and it is compared with the value used in step 2.

5) Steps 2–4 may be repeated according to a convergence criterion.

Numerical Solution Procedure

Method of Solution

The finite-difference method used to solve the equations entails subdividing the calculation domain into a number of finite volumes or "cells." The solution algorithm was embodied in a version of the TEACH program[20] for three-dimensional recirculating flows. The convection terms were discretized by the hybrid central/upwind method.[21] The velocities and pressures are calculated by a variant of the SIMPLE algorithm.[22] The solution of the individual equations sets was obtained by a form of Gauss-Seidel line-by-line iteration.

Computational Details

The equations presented in the preceding section, together with appropriate boundary conditions, have been applied to the geometry shown in Fig. 1. A grid of $19 \times 17 \times 18$ nodes (r,θ,x directions) was used. The number of iterations required for a convergent solution was approximately 220, which corresponds to approximately 50 h of CPU time in a Micro VAX II. Convergence was achieved when the normalized residuals for the three momentum equations and mass conservation were less than 2×10^{-3}.

The iterative procedure for the heat-transfer calculation was embodied in the SIMPLE algorithm. This calculation was performed only after the residuals of the main variables had attained the value 8×10^{-3}, and for every five iterations. As described in the preceding section, this iterative process for the heat-transfer calculation consists of: 1) starting from a guessed liner wall temperature (flame side); 2) calculating internal radiation and convection; and 3) the liner wall temperature (coolant side) and, again, the liner wall temperature (flame side), which will correct the guessed value. This iterative procedure was applied to each wall boundary cell of the grid. The difference between the liner temperature (flame side) for two successive iterations was calculated for all of the boundary cells. The process was considered to have "converged" if the mean value of these differences, ΔT_{mean}, would be less than or equal to 10 K and the maximum value, $\Delta T_{\max}$, was less than or equal to 50 K. Table 2 summarizes the evolution of ΔT_{mean} and $\Delta T_{\max}$, as well as the number of iterations required to solve the heat balance equations [Eqs. (13)] for case 3 (25 bar). When the algorithm is called for the first time (iteration 180 of the SIMPLE algorithm), six iterations were required to satisfy the conditions $\Delta T_{\text{mean}} \leqq 10$ K and $\Delta T_{\max} \leqq 50$ K. Later, however, only one iteration was necessary to satisfy these requirements and the values of ΔT_{mean} and $\Delta T_{\max}$ diminish continuously. As Table 2 shows, the converged solution satisfies the conditions $\Delta T_{\max} \leqq 1$ K and $\Delta T_{\text{mean}} \leqq 0.2$ K. However, if such a criterion had been chosen, the number of iterations required in previous iterations of the SIMPLE algorithm would have increased markedly.

When treatment of the radiation heat transfer is included, the calculation time per iteration increases about 50% if only

Table 2 Evolution of the control parameters for the liner temperature calculation algorithm

Iteration no. (SIMPLE algorithm)	Number of iterations required to solve Eq. (13)	$\Delta T_{\max}$, K	ΔT_{mean}, K
180	6	25.4	8.4
185	1	14.1	5.9
190	1	9.3	3.6
195	1	6.0	2.3
200	1	4.0	1.5
205	1	2.7	0.9
210	1	1.8	0.6
215	1	1.2	0.4
220	1	0.9	0.2

one iteration is required to solve the heat balance equations [Eqs. (13)]. This increase is essentially due to the time required to evaluate the internal radiation R_1 by the discrete transfer method. However, the number of iterations in which the calculation of radiation heat transfer is performed is quite low, because this procedure was performed only after residuals of the main variables had attained the value 8×10^{-3} for every five iterations. Therefore, the global computation time of the present calculations is only 3% higher when compared with calculations neglecting radiation heat transfer.

Discussion of Results

Figure 2 shows the temperature distribution of the backplate (Fig. 2a), inner annulus wall (Fig. 2b), and outer annulus wall (Fig. 2c) for the conditions identified in Table 1 as case 1 ($p = 5$ bar). The film-cooling air near the outer and inner annulus walls can be identified in the backplate temperature distribution by the presence of the two lines corresponding to low temperature (500 K and 600 K) near and parallel to the annulus walls. In the middle of the backplate, there is a region of high gradients that is the center of combustion activity. Near the symmetry planes, the temperature is higher (800 K) because of the recirculation of hot gases.

The temperature distribution of the two annulus walls (Figs. 2b and 2c) reflects the distribution of the cooling holes. The temperature levels increase from the burner side to the exit side. Until reaching the location of the second row of holes, the film-cooling air protects the walls, avoiding the occurrence of high temperature. However, due to diffusion, the cool air will tend to mix with the mainstream, and the hot gases from the mainstream will tend to mix with the cool air, increasing its temperature. The highest temperatures (800 K) in the annulus walls occur near the two corners formed between the exit plane and the symmetry planes. This is because the middle region of the exit plane is under the cooling effect of the dilution air from the second row of holes. It is worth noting that, in this case, the maximum wall temperature is about 800 K and the maximum temperature difference is on the order of 300 K.

Figure 3 displays the radiation heat-transfer contours to the backplate and to the inner and outer annulus walls for a working pressure of 5 bar (case 1). The heat flux to the three walls is rather uniform. For the backplate (Fig. 3a), the radiative heat flux wavers about a value of 25 kW/m^2, although near the entrance of the film-cooling air the heat flux attains a value of 50 kW/m^2. For the annulus walls, it can be seen that the higher values of the radiative heat fluxes can be found in the intermediate region of the combustor between the burner and exit planes. This is a consequence of the higher temperature of the gases in this region, since after the second row of holes, the temperature of the gases decreases because of the effect of the dilution air. The heat transfer to the inner annulus wall reflects the distribution of the cooling holes. The heat flux through the holes is more than to the walls; however, since the holes cover less than 5% of the total wall area, this fact is not significant.

Figure 4 shows the gas field temperature on a plane perpendicular to the axis of symmetry of the combustor after the second row of holes near the exit for $p = 5$ bar. The feature of dilution air intrusion is still identified at this location, where cooler air penetration again follows the pattern expected from the hole geometry with one cool region near the bottom wall and one near the upper wall. It is known that a uniform exit temperature distribution would be considered ideal in order to maximize the life of the turbine blades and nozzle guidevanes. However, as can be seen for the present case, the distribution of temperature at the combustor exit is far from uniform, as usually happens in all modern high-performance engines.

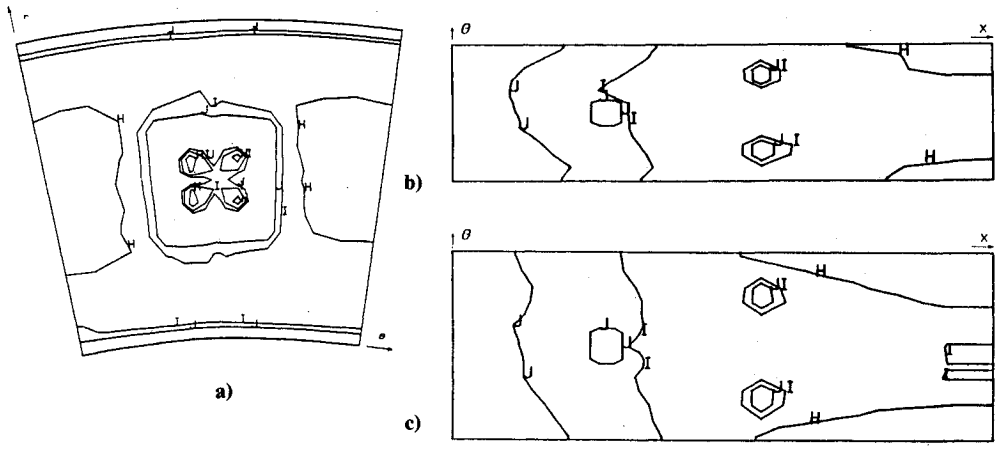

Fig. 2 Wall temperature distribution ($p = 5$ bar): a) combustor backplate; b) inner annulus wall; and c) outer annulus wall [contour levels (K): H = 800; I = 600; and J = 500].

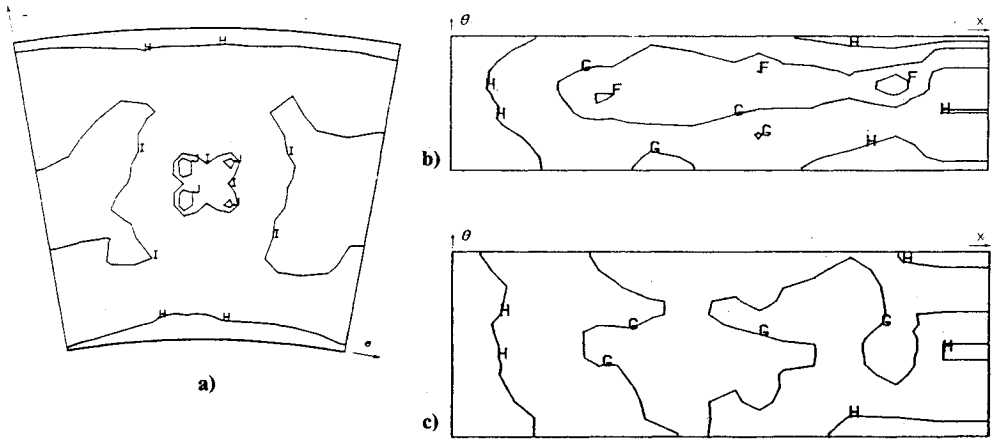

Fig. 3 Radiative wall heat fluxes ($p = 5$ bar): a) combustor backplate; b) inner annulus wall; and c) outer annulus wall [contour levels (kW/m^2): F = 150.0; G = 100.0; H = 50.0; I = 25.0; and J = 10.0].

Figures 5 and 6 show the temperature distribution and the radiative heat flux distribution to the combustor walls for a working pressure of 15 bar (case 2). Figure 7 shows the gas field temperature distribution at a plane near the exit for the same pressure. For a pressure of 25 bar (case 3), the temperature and radiative heat flux distributions are shown in Figs. 8 and 9, respectively. Comparing the results for the different working pressures, it can be concluded that the distributions are qualitatively similar. However, the effect of the presence of the cooling holes in the temperature and flux distributions of the annulus walls is more pronounced for higher pressures. The levels of temperature and fluxes increase with pressure because of the increase of the temperature of the gases and gas emissivity. The highest wall temperature observed in all cases is on the order of 1100 K. To ensure a satisfactory liner life, it is important to keep temperatures down to an acceptable level. It is generally recognized that, for the commonly used materials, the maximum temperature of the liner should not greatly exceed 1100 K.[1] In the cases investigated, temperatures of this order of magnitude occur only for pressures of 15 and 25 bar near the exit plane where the film cooling is no longer effective.

Figure 10 shows the total heat-transfer contours to the backplate, inner and outer annulus walls for a pressure of 25 bar. The convective fluxes to the holes were not calculated. Therefore, the distribution of heat fluxes near the holes is meaningless. Comparing Figs. 9 and 10, it can be concluded that radiation is more important in the primary zone and convection is more important in the dilution zone. The temperature of the film-cooling air is kept low in the primary zone. Therefore, the convective heat transfer to the liner in this region will be small. As the temperature of the film-cooling air increases, the convective heat transfer to the liner will also increase.

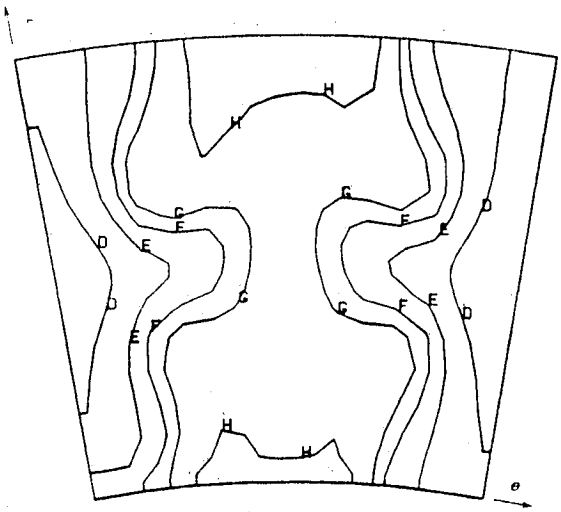

Fig. 4 Gas field temperature for the plane: $x = 0.32$ m, $p = 5$ bar [contour levels (K): D = 1500; E = 1250; F = 1100; G = 1000; and H = 800].

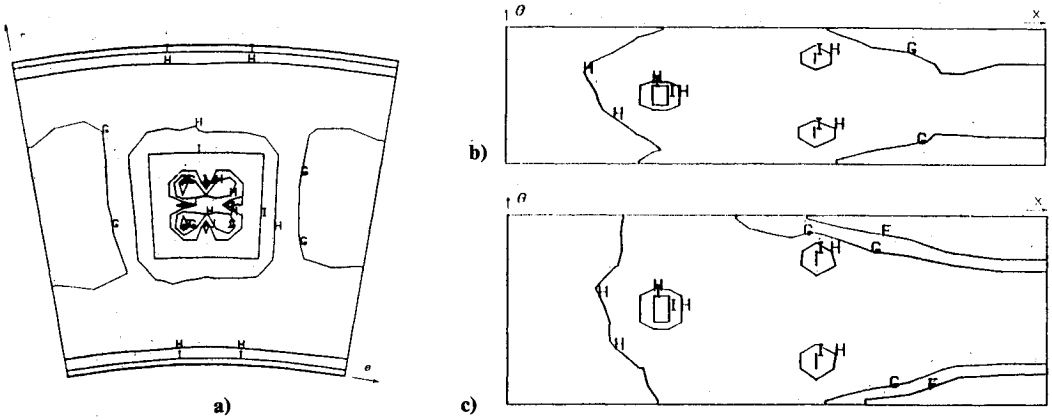

Fig. 5 Wall temperature distribution (p = 15 bar): a) combustor backplate; b) inner annulus wall; and c) outer annulus wall [contour levels (K): F = 1100; G = 1000; H = 800; I = 600; and J = 500].

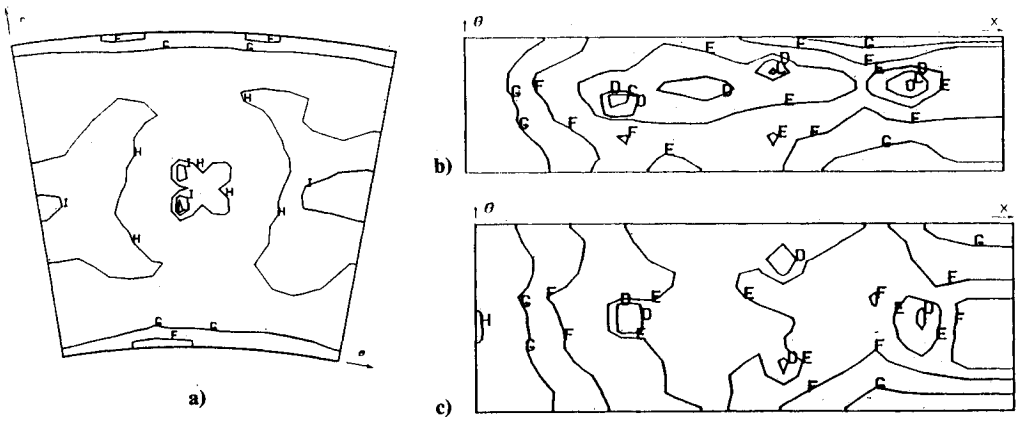

Fig. 6 Radiative wall heat fluxes (p = 15 bar): a) combustor backplate; b) inner annulus wall; and c) outer annulus wall [contour levels (kW/m^2): C = 300.0; D = 250.0; E = 200.0; F = 150.0; G = 100.0; H = 50.0; I = 25.0; and J = 10.0].

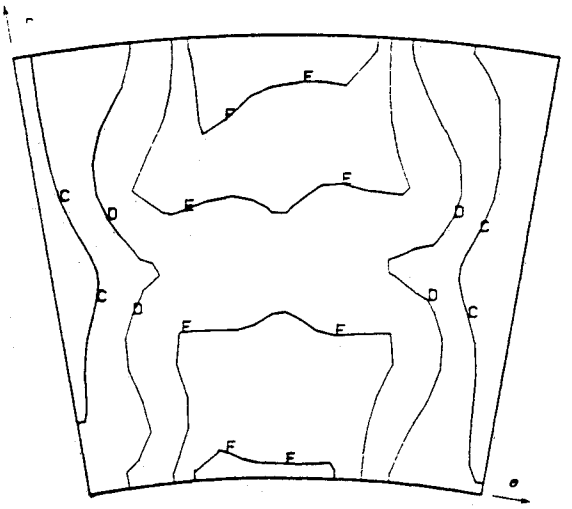

Fig. 7 Gas field temperature for the plane: $x = 0.32$ m, $p = 15$ bar [contour levels (K): C = 1750; D = 1500; E = 1250; and F = 1100].

Figure 11 shows temperature contours for a plane located near the exit of the combustor. The features of the contours are similar to those of Figs. 4 ($p = 5$ bar) and 7 ($p = 15$ bar) because the location is the same.

Table 3 shows the radiative, convective, and total heat fluxes to the walls for the three combustor pressures investigated. The values of the heat fluxes presented in this table are referred to all 18 sectors of the combustor. As can be seen, the radiative and convective fluxes are small. The small convective fluxes can be justified by the streams of cooling air close to the annulus walls. Although this cooling air deteriorates the temperature pattern factor, reduces combustion efficiency, and contributes to the presence of pollutants in the exhaust gases,[6] its presence is required to reduce wall temperature. Both radiative and convective fluxes increase with pressure, attributed mainly to the increase of inlet air temperature and gas emissivity. The ratio of these fluxes to the energy supplied to the combustor is about 1%, which is almost the same for the three cases studied. However, convective fluxes are slightly greater than radiative ones.

In our calculations, no attempt has been made to account for the presence of soot. Soot would enhance radiative heat transfer mainly at high pressures. However, the results of Naegeli et

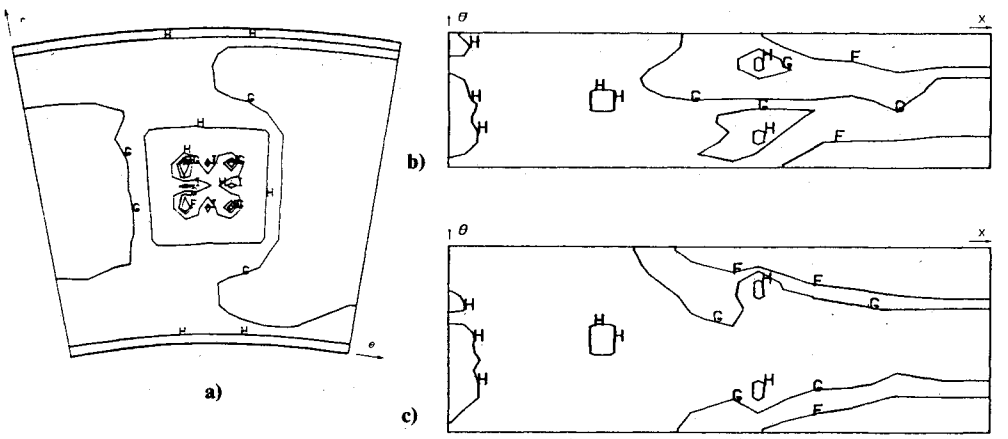

Fig. 8 Wall temperature distribution ($p = 25$ bar): a) combustor backplate; b) inner annulus wall; and c) outer annulus wall [contour levels (K): F = 1100; G = 1000; H = 800; and I = 600].

Table 3 Heat fluxes to the walls, kW

Combustor pressure	Wall considered	Radiative heat transfer	Radiative heat transfer/energy supplied to combustor, %	Convective heat transfer	Convective heat transfer/energy supplied to combustor, %	Total heat transfer	Total heat transfer/energy supplied to combustor, %
5 bar	Combustor backplate	6.4	0.07	9.7	0.11	16.1	0.18
	Inner annulus wall	45.4	0.49	49.0	0.53	94.4	1.02
	Outer annulus wall	68.0	0.74	72.5	0.78	140.5	1.52
	Total	119.8	1.30	131.2	1.42	251.0	2.72
15 bar	Combustor backplate	12.3	0.07	20.3	0.11	32.6	0.18
	Inner annulus wall	88.4	0.48	116.5	0.63	204.9	1.11
	Outer annulus wall	131.6	0.71	172.1	0.93	303.7	1.65
	Total	232.3	1.26	308.9	1.68	541.2	2.94
25 bar	Combustor backplate	13.4	0.06	25.6	0.10	39.0	0.16
	Inner annulus wall	96.1	0.39	120.8	0.49	216.9	0.88
	Outer annulus wall	146.2	0.59	179.8	0.73	326.0	1.32
	Total	255.7	1.04	326.2	1.32	581.9	2.36

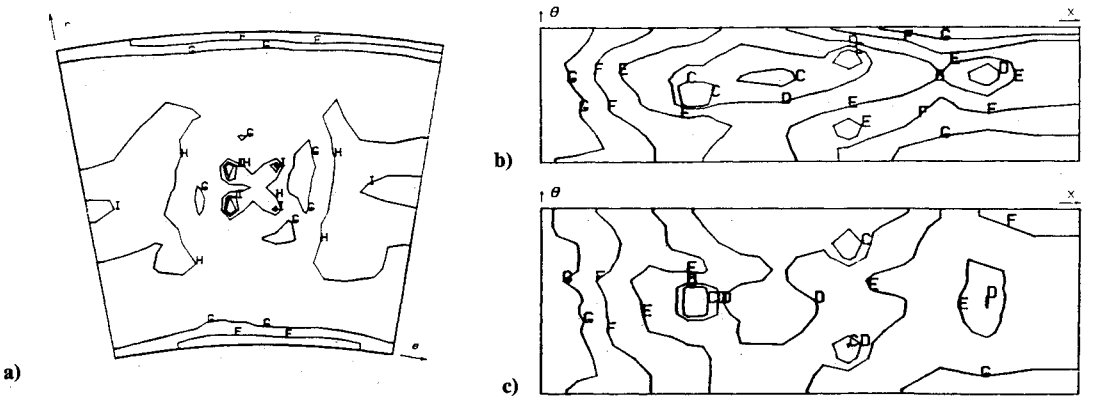

Fig. 9 Radiative wall heat fluxes (p = 25 bar): a) combustor backplate; b) inner annulus wall; and c) outer annulus wall [contour levels (kW/m^2): C = 300.0; D = 250.0; E = 200.0; F = 150.0; G = 100.0; H = 50.0; I = 25.0; and J = 10.0].

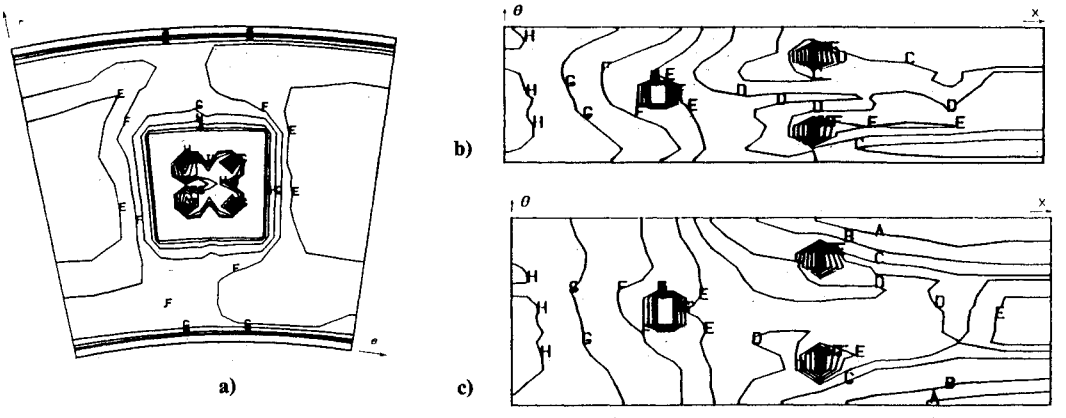

Fig. 10 Total wall heat fluxes (p = 25 bar): a) combustor backplate; b) inner annulus wall; and c) outer annulus wall [contour levels (kW/m^2): A = 500.0; B = 400.0; C = 300.0; D = 250.0; E = 200.0; F = 150.0; G = 100.0; H = 50.0; I = 25.0; and J = 10.0].

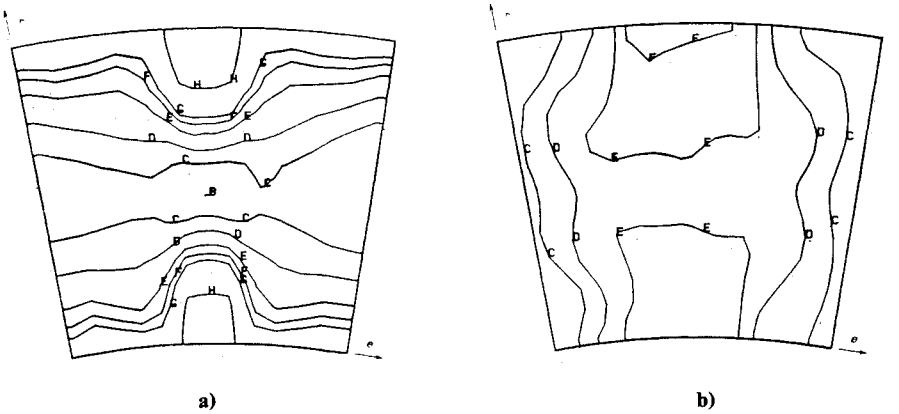

Fig. 11 Gas field temperature: p = 25 bar, plane x = 0.320 m [contour levels (K): B = 2000; C = 1750; D = 1500; E = 1250; F = 1100; G = 1000; nd H = 800].

al.[18] showed that, within the pressure range of interest for gas turbines (5–25 bar), sooting tendency is very dependent on fuel type and composition, and hydrogen content or C/H ratio is the principal correlating parameter for sooting tendency. The fuel considered in the present work, propane, has a high hydrogen content, yielding a low propensity toward soot formation.

Concluding Remarks

The present paper describes a prediction procedure for the calculation of the flow, heat-transfer, and combustion processes inside a three-dimensional can combustor chamber of a gas turbine. The incorporation into the computational scheme of a technique for calculating the distribution of temperature and heat fluxes in the liner represents the main contribution of this paper. It is believed that is the first time that the temperature and heat flux distributions of the liner were calculated. All of the previous works have imposed the liner temperature. The calculation method outlined in the present paper constitutes the only correct way to calculate the liner temperature (a heat balance to the liner linking the heat-transfer processes occurring in the combustion chamber with the heat-transfer processes occuring in the outer annular region). The present model constitutes an accurate and flexible prediction procedure for the calculation of the heat flux distributions within the combustion chambers. The use of this prediction procedure can yield improved linear durability in future designs by prescribing optimum arrangements for the quantity and distribution of film-

cooling air. This approach also can lead to significant reductions in the time and cost of liner development.

The influence of working pressure on heat transfer was investigated by comparing the radiative, convective, and total heat fluxes, and the temperature distribution of the liner for three different working pressures: 5, 15, and 25 bar. Both radiative and convective fluxes increase with pressure, attributed mainly to the increase of inlet air temperature and gas emissivity. The ratio of the fluxes to the energy supplied to the combustor is very small. However, the accurate assessment of the flux distribution is an essential prerequisite for the prediction of the liner temperature distribution and liner life.

Acknowledgments

The authors wish to thank Dr. J. McGuirk for his useful suggestions on this work. The financial support of Instituto Nacional de Investigação Científica and of Calouste Gulbenkian Foundation, Lisbon, is acknowledged.

References

[1]Lefebvre, A. H., *Gas Turbine Combustion*, McGraw-Hill, New York, 1983, Chaps. 1 and 8.

[2]Jones, W. P., Clifford, W. C., Priddin, C. H., and De Chair, R., "A Comparison Between Predicted and Measured Species Concentrations and Velocities in a Research Combustor," *Proceedings of the AGARD 50th Meeting*, Paper 41, 1977, pp. 41-1–41-16.

[3]Jones, W. P. and Priddin, C. H., "Prediction of the Flow Field and Local Gas Composition in Gas Turbine Combustors," *Proceedings of the 17th Symposium (International) on Combustion*, The Combustion Inst., Pittsburgh, PA, 1979, pp. 399–409.

[4]Jones, W. P. and McGuirk, J., "Mathematical Modelling of Gas Turbine Combustion Chambers," *Proceedings, AGARD–275*, Paper 4, 1980, pp. 4-1–4-10.

[5]Coupland, J. and Priddin, C. H., "Modelling the Flow and Combustion in a Production Gas Turbine Combustor," *Proceedings of the 5th Turbulent Shear Flow Symposium*, edited by F. Durst et al., Springer-Verlag, New York, 1986.

[6]Lefebvre, A. H., "Flame Radiation in Gas Turbine Combustion Chambers," *International Journal of Heat and Mass Transfer*, Vol. 27, Sept. 1984, pp. 1493–1510.

[7]Boysan, F., Ayers, W. H., Swithenbank, J., and Pan, Z., "Three-Dimensional Model of Spray Combustion in Gas Turbine Combustors," *Journal of Energy*, Vol. 6, No. 6, 1982, pp. 368–375.

[8]Sampath, S. and Ganesan, V., "Numerical Prediction of Flow and Combustion in Three-Dimensional Gas Turbine Combustors," *Journal of the Institute of Energy*, Vol. 11, March 1987, pp. 15–28.

[9]Lockwood, F. C., McGuirk, J. J., and Shah, N. G., "Radiation Transfer in Gas Turbine Combustors," AIAA Paper 83–1506, June 1983.

[10]Lockwood, F. C. and Shah, N. G., "A New Radiation Solution Method for Incorporation in General Combustion Prediction Procedures," *Proceedings of the 18th Symposium (International) on Combustion*, The Combustion Institute, Pittsburgh, PA, 1981, pp. 1405–1414.

[11]Gordon, S. and McBride, B. J., "Computer Program for the Calculation of Complex Chemical Equilibrium Compositions," NASA SP–273, 1971.

[12]Carvalho, M. G., Durão, D. F. G., and Lockwood, F. C., "Computation of Thermal Radiation for Gas Turbine Conditions," *Proceedings of the 65th AGARD/PEP Symposium*, Bergen, CP–390, Paper 20, 1985, pp. 20-1–20-7.

[13]Launder, B. E. and Spalding, D. B., *Mathematical Models of Turbulence,* Academic, New York, 1972.

[14]Godoy, S., "Turbulent Diffusion Flames," Ph.D. Thesis, Univ. of London, England, UK, 1982.

[15]Carvalho, M. G., "Computer Simulation of a Glass Furnace," Ph.D. Thesis, London Univ., England, UK, 1983.

[16]Lockwood, F. C. and Naguib, A. S., "The Prediction of the Fluctuations in the Properties of Free, Round Jet, Turbulent Diffusion Flames," *Combustion and Flame*, Vol. 24, Feb. 1975, pp. 109–124.

[17]Truelove, J. S., "A Mixed Grey Gas Model for Flame Radiation," AERE Harwell, UK, Rept. HL 76/3448/KE, 1976.

[18]Naegeli, D. W., Dodge, L. G., and Moses, C. A., "Effects of Flame Temperature and Fuel Composition on Soot Formation in Gas Turbine Combustors," *Combustion Science and Technology*, Vol. 35, Dec. 1983, pp. 117–131.

[19]Schlichting, H., *Boundary Layer Theory*, McGraw-Hill, New York, 1968, Chap. 23.

[20]Gosman, A. D., Humphrey, J. A. C., and Vlachos, N. S., "TEACH-3E: A General Computer Program of Three-Dimensional Recirculating Flows," Department of Mechanical Engineering, Imperial College, England, UK, Rept. CHT/76/10, 1976.

[21]Spalding, D. B., "A Novel Finite Difference Formulation for Differential Expressions Involving Both First and Second Derivatives," *International Journal of Numerical Methods in Engineering*, Vol. 4, July–Aug. 1972, p. 551.

[22]Caretto, L. S., Gosman, A. D., Patankar, S. V., and Spalding, D. B., "Two Calculation Procedures for Steady, Three-Dimensional Flows with Recirculation," *Proceedings of the 3rd International Conference on Numerical Methods in Fluid Dynamics*, Springer-Verlag, New York, 1972, p. 60.